Accurate power sharing for islanded DC microgrids considering mismatched feeder resistances

Mohammed, Nabil; Callegaro, Leonardo; Ciobotaru, Mihai; Guerrero, Josep M.

Published in:
Applied Energy

DOI (link to publication from Publisher):
10.1016/j.apenergy.2023.121060

Publication date:
2023

Document Version
Publisher's PDF, also known as Version of record

Applied Energy 340 (2023) 121060

Contents lists available at ScienceDirect

Applied Energy

journal homepage: www.elsevier.com/locate/apenergy

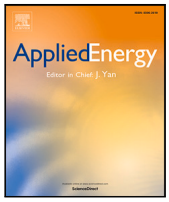

Accurate power sharing for islanded DC microgrids considering mismatched feeder resistances

Nabil Mohammed [a,*], Leonardo Callegaro [b], Mihai Ciobotaru [b], Josep M. Guerrero [c]

[a] Department of Electrical and Computer Systems Engineering, Monash University, VIC 3800, Australia
[b] School of Engineering, Macquarie University, NSW 2113, Australia
[c] Department of Energy Technology, Aalborg University, Aalborg 9220, Denmark

ARTICLE INFO

Keywords:
Boost converter
DC microgrid
Mismatched resistances
Power sharing
Resistance measurement
Virtual resistance

ABSTRACT

Accurate load power sharing and bus voltage regulation are two critical control objectives for ensuring power quality and reliable operation of DC microgrids. Although regulating the DC Bus voltage can be achieved by adopting an external secondary control loop, inaccurate load power/current sharing among converters is a prominent issue due to feeder resistances mismatch. This can lead to undesired overloading of converters, triggering over-current protection relays, and potentially resulting in cascading failure of the whole system. Existing literature uses virtual resistance techniques to improve the power sharing accuracy; however, so far, no explicit relation between the values of the virtual resistances and the feeder resistances mismatch has been formulated, opening the possibility to enhance power sharing even further. Therefore, this paper proposes an accurate power sharing strategy in which the virtual resistances are chosen to account for the feeder resistances mismatch. The proposed technique relies on the optimal tuning of the virtual resistance assigned to the local controller of each converter. An online estimation algorithm of the physical feeder resistances, required for virtual resistance tuning, is embedded into the control loop of each converter. Thus, prior information about the feeder resistances in the design stage is not required. The proposed approach is validated through simulation and experimental results from a Hardware-in-the-Loop setup of a typical islanded DC microgrid. The results demonstrate the approach merits, achieving accurate power sharing among converters and ensuring robust operation, even in scenarios involving communication failures.

1. Introduction

Power electronics is a crucial technology that enables the ongoing transition to a power system based on renewables and distributed generation, including the integration of low voltage AC and DC microgrids (DC MG)[1,2]. Microgrids aggregate sources and loads of different natures into a single dispatchable system, and they can operate interconnected to a larger AC or DC network or in standalone mode. The operation of AC microgrids is affected by power quality issues, such as harmonics, reactive power flow, frequency synchronization, and transformer inrush current, which can only be mitigated by using complex control algorithms. In contrast, DC microgrids do not have these issues, resulting in a simpler control[3]. Nevertheless, research on DC MG has been very dynamic in the last decade, addressing architectures, control strategies, stability, protection, and applications [4–7].

This paper concerns the islanded operation mode of DC MG, where the two common control objectives are load sharing (power or current) and DC Bus voltage regulation, traditionally achieved using droop algorithms at the primary control level [8]. Droop control is implemented at the converter level and ensures power sharing and stable operation of the DC MG without the need for communication links [4,9]. Despite these advantages, droop control also has some deficiencies. Firstly, it fails to regulate the DC Bus voltage to its reference due to steady-state output voltage deviations in each converter [8], caused by voltage drops across feeder impedances while supplying the required load current. Secondly, droop control guarantees load power sharing only if the feeder resistances between the DC–DC converters and the common DC Bus are identical [10], which is unlikely to occur in practice. In summary, droop control has an inherent tradeoff between voltage regulation and load power sharing, which is strongly influenced by line resistances [11,12].

On the one hand, to address the issue of DC Bus voltage regulation in DC MG, an external control layer can be implemented using either centralized or distributed architecture [9]. In the centralized control strategy, a secondary outer layer of control is typically used. The outer microgrid central controller (MGCC) senses the DC Bus voltage

* Corresponding author.
E-mail address: nabil.mohammed@ieee.org (N. Mohammed).

https://doi.org/10.1016/j.apenergy.2023.121060
Received 2 January 2023; Received in revised form 21 February 2023; Accepted 25 March 2023
Available online 5 April 2023

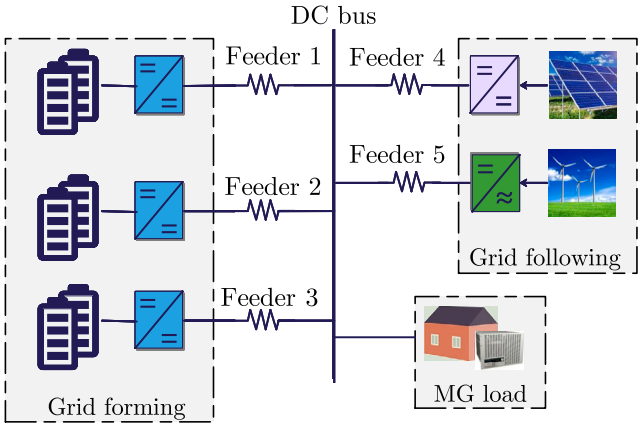

Fig. 1. Typical configuration of an islanded DC microgrid (the secondary controller is not shown).

and compares it to the reference value. A PI controller inside the MGCC processes the voltage error, and its output is communicated to the local controller of each converter via a link [9]. Thus, each converter can modify its output voltage reference in the primary (local) controller to eliminate the DC Bus voltage deviation identified by the secondary (common) controller. As the centralized approach reduces reliability due to the existence of a single point of failure [8,13], the distributed control [13–16], sparse communication network and consensus-based algorithm [10,17,18] are proposed to compensate the voltage deviations in DC MG. However, these control techniques still require communication links to exchange information between each converter with every other (or neighboring) converters in the microgrids to determine the appropriate voltage-shifting quantity by calculating the average values of the DC Bus voltage and load current.

On the other hand, the problem of inaccurate load power sharing between converters is mitigated if the effects of line resistance mismatches are compensated [8]. Fig. 1 reports an example where multiple battery-powered grid-forming DC–DC converters are connected in parallel to provide sufficient capacity to a DC microgrid. Accurate power sharing among these converters is crucial to prevent uneven discharging of the battery sets [19–21] and to maximize the system lifespan. Traditionally, achieving accurate power sharing involves constant voltage shifting of the converter output or adjusting the droop coefficients of the converter [17,22–24]. In [22], converters share information on droop resistance, output voltage, and current. Each converter then calculates the average value of these parameters to apply voltage shifting and adjust the converter droop resistance. However, this approach requires high-bandwidth bidirectional communication between all converters, which is a drawback. To improve flexibility and resiliency against communication failures, sparse communication and cooperative control are proposed in [17,23].

Nevertheless, correcting DC Bus voltage deviations is a complex process that relies on a sophisticated structure. A decentralized voltage restoration strategy was proposed in [24], which adds voltage-shifting compensation to the unit's voltage droop control reference to ensure zero steady-state error. However, this technique raises concerns regarding line resistances, circulating currents, and the absence of a consistent current sharing strategy. In [25], an enhanced droop control for islanded DC microgrids is introduced based on virtual voltage, which replaces the actual output voltage. Although this approach ensures equal power sharing between converters, it requires full information on all DC–DC converters in the microgrids, including the number of converters and the actual output voltages, to select the average value of each DG actual output voltage as the virtual voltage.

All of the studies mentioned above achieve DC Bus voltage deviations and accurate power sharing between converters through droop coefficient adjustment/shifting, virtual resistance, and virtual voltage. However, none of them discuss how to assign the optimal value for the virtual resistance of each converter. This is an important consideration as there is an inherent trade-off between power sharing and voltage deviations. For instance, a high virtual resistance value ensures good power sharing but leads to larger voltage deviations, which cause further voltage degradation [26]. Moreover, accurate power sharing between converters based on droop coefficient adjustment is not guaranteed due to the inevitable differences in line resistance in the distributed DC microgrid [10,27,28]. Finally, the literature mentioned above does not establish an explicit relation between the value of the virtual resistances assigned to each converter and the mismatched values between different feeder resistances, which are the main cause of inaccurate current or power sharing..

This paper proposes a strategy for accurate power sharing in islanded DC microgrids. The proposed strategy considers the mismatched interconnecting feeder resistances, which are the main cause of line voltage drops and inaccurate proportional power and current sharing between the DC–DC converters, to calculate the optimal values for the virtual resistances of these converters. The presented control is simple yet effective and is implemented into the conventional centralized DC microgrid structure. Its main advantages are:

1. Achieving accurate power sharing in the presence of mismatched feeder resistances by optimally tuning the virtual resistance of each converter to fully mitigate the negative impact of mismatched values in the physical feeder resistances.
2. Estimating the physical feeder resistances in real-time using the recursive least squares algorithm to be used in the virtual resistance optimal tuning. Hence, prior information on the feeder resistances in the design stage is not required.
3. Preventing unnecessary large voltage deviations in the DC microgrid, thereby increasing efficiency and reliability.
4. Simplicity and flexibility since it is software-based and does not require extra hardware. It is also suitable for upgrading existing microgrids.
5. Reducing the dependence on communication links since it ensures accurate load power sharing even under permanent communication failure between the MGCC and the converters, making it a fault-tolerant and reliable control approach.

The remainder of the paper is organized as follows: Section 2 presents the fundamental operational concepts of islanded DC microgrids. Section 3 illustrates the proposed converter power sharing strategy based on virtual resistance. Section 4 presents simulations and hardware-in-the-loop (HIL) experimental results to validate the performance of the proposed control scheme. Section 5 concludes the paper.

2. Fundamental operational concepts of islanded DC microgrids

Fig. 2 depicts the equivalent model of an islanded DC microgrid consisting of two DC–DC converters, represented as dependent voltage sources, and a microgrid central load. To effectively control the DC Bus voltage and converter power sharing in such a microgrid, each converter employs a cascaded control scheme comprising an inner current loop and an outer output voltage loop, as described in [9]. The reference for the output voltage controller of each converter is adjusted using input from the external voltage controller or set point, which is common to all grid forming converters shown in Fig. 1.

In DC microgrids, it is desired that the load power is shared between converters proportionally to their power rating. To achieve this objective, an additional outer power droop control loop is usually implemented [4]. Hence, equal power sharing is necessary among the grid forming inverters to provide sufficient capacity and prevent over discharging of individual battery sets [19–21]. If the DC–DC converters have equal power ratings, even load sharing can be achieved without

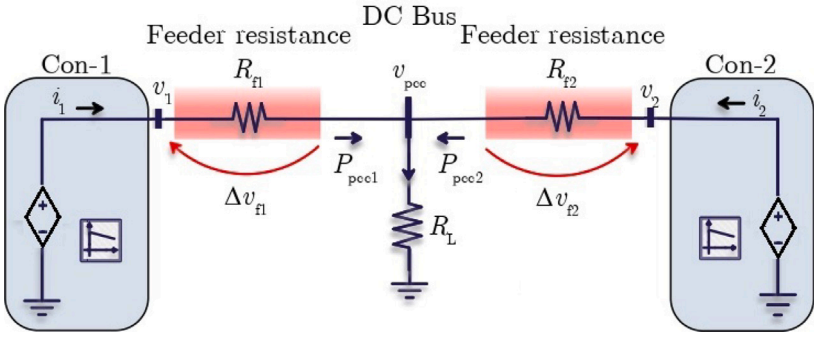

Fig. 2. Equivalent model of an islanded DC microgrid illustrating load-sharing between two converters (without virtual resistance).

implementing the power droop control loop, which is the scenario considered in this paper. When all the DC–DC converters have identical power ratings and the feeder resistances are equal, they should provide equal power to the load. However, the equality of feeder resistances is an ideal condition, and in reality, mismatched feeder resistances lead to inaccurate power sharing between converters. This can result in undesired circulating currents between converters, overloading of specific converters, and triggering of over-current protection relays, leading to potential cascading failure of the entire system [29,30]. Therefore, the principles that govern power sharing among identical converters, taking into account the impact of feeder resistance, are quantified in the following section.

2.1. Accurate power sharing with equal feeder resistances

In the circuit of Fig. 2, the microgrid load current is:

$$i_L = i_1 + i_2 = \frac{v_1 - i_L R_L}{R_{f1}} + \frac{v_2 - i_L R_L}{R_{f2}} \tag{1}$$

According to (1), the portions of load current delivered by converter 1 (i_1) and converter 2 (i_2) are directly influenced by the resistance values of feeder 1 (R_{f1}) and feeder 2 (R_{f2}). The voltage drops across the resistances of feeder 1 and feeder 2 can be respectively expressed as:

$$\begin{cases} \Delta v_{f1} = R_{f1} i_1 \\ \Delta v_{f2} = R_{f2} i_2 \end{cases} \tag{2}$$

Assuming fixed converter output voltages v_1 and v_2 with $v_1 = v_2$, two operational scenarios determine the accuracy of power sharing between the two converters. The first scenario is when both converters are identical ($P_{rated1} = P_{rated2}$) and the feeder resistances are also identical ($R_{f1} = R_{f2}$), the power sharing is given by:

$$\begin{cases} P_{rated1} = P_{rated2} \\ R_{f1} = R_{f2} \end{cases} \Longrightarrow \begin{cases} \Delta v_{f1} = \Delta v_{f2} \\ i_1 = i_2 \\ P_{pcc1} = P_{pcc2} \end{cases} \tag{3}$$

where P_{pcc1} and P_{pcc2} represent the power delivered by each converter to the load connected to the common DC Bus, i.e., the point-of-common-coupling (PCC). The second scenario, which considers feeders with different resistance values, will be discussed next.

2.2. Inaccurate power sharing with unequal feeder resistances

Assuming, for simplicity, that the resistance of feeder 1 is greater than that of feeder 2 ($R_{f1} > R_{f2}$), the resistance mismatch between the two feeders can be expressed as:

$$\delta R_f = R_{f1} - R_{f2} \tag{4}$$

Likewise, the voltage drop mismatch between the two feeders can be expressed as:

$$\delta V = \Delta v_{f1} - \Delta v_{f2} = f(\delta R_f) \tag{5}$$

with $R_{f1} > R_{f2}$, (5) indicates that the voltage drop across feeder 1 (Δv_{f1}) is greater than the voltage drop across feeder 2 (Δv_{f2}) by δV. Referring back to (1) (with constant $v_1 = v_2$), it is concluded that converter 1 will supply less current and, consequently, less power to the load than converter 2, leading to inaccurate power sharing between the two identical converters. The impact of unequal feeder resistances on power sharing of the two identical DC–DC converters can be summarized in as follows:

$$\begin{cases} P_{rated1} = P_{rated2} \\ R_{f1} > R_{f2} \end{cases} \Longrightarrow \begin{cases} \Delta v_{f1} > \Delta v_{f2} \\ i_1 < i_2 \\ P_{pcc1} < P_{pcc2} \end{cases} \tag{6}$$

From (1) to (6), it is evident that unequal feeder resistances are the primary cause of uneven power sharing among DC–DC converters in DC microgrids. A similar conclusion was drawn in [31] for AC microgrids, where unequal feeder impedance components (resistance and inductance) negatively impacted the accuracy of power sharing between DC–AC converters. While active load power sharing in AC microgrids remains unaffected by mismatched feeder impedances, reactive power is highly sensitive to such operating scenarios [31,32].

2.3. Traditional virtual resistance approach

As illustrated above, accurate power sharing among DC–DC converters cannot be guaranteed under unequal feeder resistances when the conventional control loops are being adopted. Hence, an effective technique called virtual resistance (R_v) was discussed in [9].

Considering the DC microgrid shown in Fig. 2, whose load sharing is described by (1), the idea is to adjust output voltage of each converter to compensate for the mismatch in the value of feeder resistance, so that the load current is equally shared between converters, i.e., $i_1 = i_2$, despite having $R_{f1} \neq R_{f2}$. Compensation of the converter output voltage occurs by means of the virtual resistance. The control law of converter j (j = 1, 2) by considering the virtual resistance and the secondary control loop is written as follows [9]:

$$v^*_{DCj} = v^*_{DC} - R_{vj} i_j + (K_{p-sec} + \frac{K_{i-sec}}{s})(v^*_{DC} - v_{pcc}) \tag{7}$$

where v^*_{DC} represents the DC Bus voltage reference, v^*_{DCj} is the output voltage reference value of converter j, and R_{vj} is the virtual resistance assigned for the converter j. K_{p-sec} and K_{i-sec} are the proportional and integral coefficients of the secondary PI compensator that is used to restore the voltage deviation in the MG, and v_{pcc} denotes the measured voltage of the DC Bus at the PCC.

Similarly, the virtual resistance R_{vj+1} assigned to converter $j+1$ drops the reference voltage of converter $j+1$ in proportion to its output current, i_{j+1}. Consequently, the negative impacts of unequal feeder

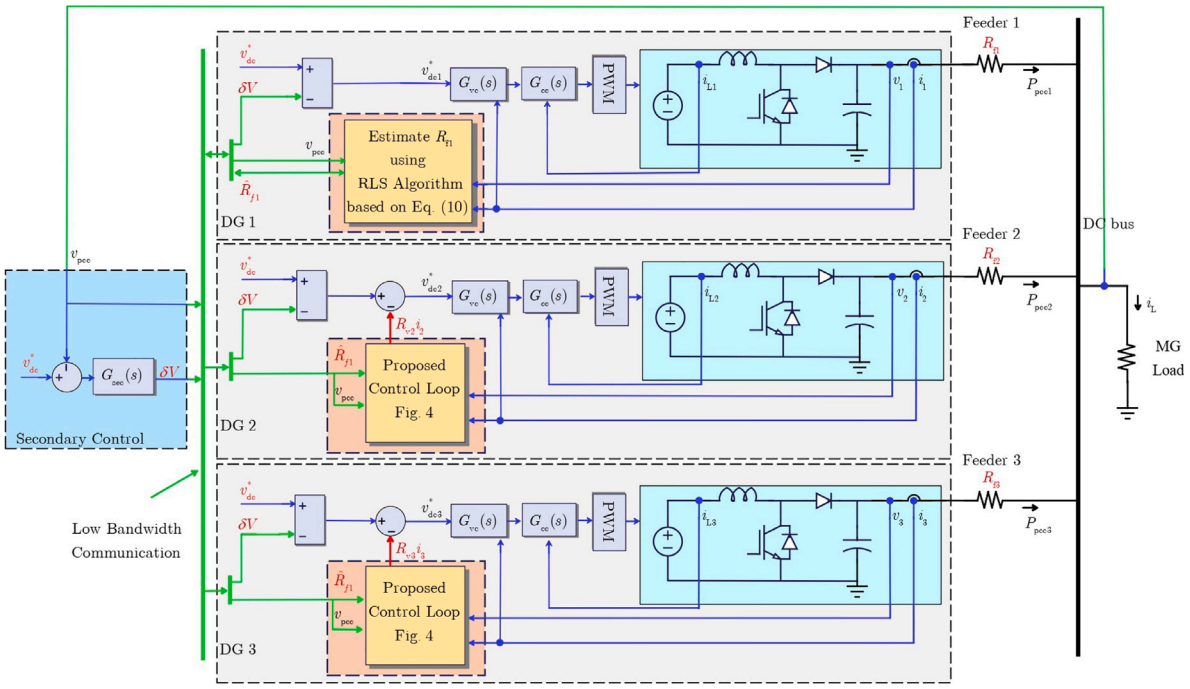

Fig. 3. A schematic diagram of the studied islanded microgrid with the proposed optimal virtual resistance for achieving accurate power sharing among three identical DC boost converters where $R_{f1} \neq R_{f2} \neq R_{f3}$.

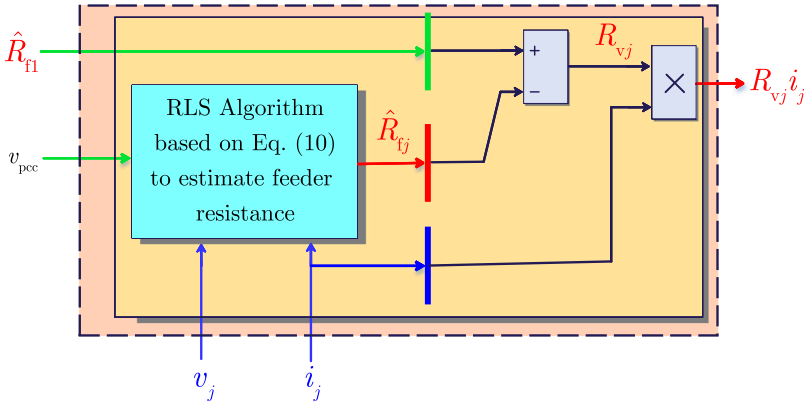

Fig. 4. Implementation of the proposed virtual resistance for the *jth* converter (j = 2, 3, ….) utilizing the online estimation of feeder resistances.

resistances on power sharing accuracy can be reduced [9]. By adjusting the output voltage of each converter to compensate for the voltage drop across its respective feeder, the power sharing accuracy is improved.

The remaining challenge in (7) is determining the optimal value of R_{vj} assigned to each converter. To fully mitigated the negative impacts of unequal feeder resistances on power sharing, optimal values for R_{v1} and R_{v2} must be chosen to compensate for the mismatched voltage drop calculated in (5). As stated earlier, previous studies (e.g., [9]) have assigned the same value of virtual resistances to all converters, greater than the maximum expected feeder resistances. However, this leads to unnecessary large voltage deviations in the DC microgrid [15], which in turn decreases its overall efficiency.

Conversely, this paper proposes a new method to determine the optimal value of virtual resistance assigned to each converter. Each virtual resistance value is calculated based on the actual value of the associated feeder resistances, which is obtained using an online estimation technique. The details of this proposed approach are explained in the following section.

3. Proposed virtual resistance control scheme

Fig. 3 depicts the detailed structure of the islanded DC microgrid under investigation. The proposed optimal virtual resistance is implemented at the primary level, locally in each converter. A common outer secondary control loop is employed to regulate the microgrid voltage (at the DC Bus) to its reference value of 400 V [9]. The control scheme of the DC microgrid uses a low-bandwidth communication channel, shown in green in Fig. 3. As shown in Fig. 4, it is noteworthy that the proposed approach for tuning the virtual resistance values relies solely on the actual feeder resistances and the converter output current, making it a generic and scalable solution suitable for DC–DC converters with small to large power ratings. A detailed explanation of the proposed control strategy follows.

3.1. Online estimation of actual feeder resistance values

To obtain a simple and reliable estimation of the feeder resistances without disturbing the system, the recursive least squares (RLS) algorithm [31,33,34] is implemented into the control loop of each

converter. This enables each converter to estimate its respective feeder resistance online using only available measurements. For example, converter 1 estimates the resistance of feeder 1, and so forth. The remainder of this section elaborates on the online resistance estimation method for feeder j by the jth converter (where $j = 1, 2, \ldots$).

The steady state output voltage of converter j can be expressed as:

$$v_j = R_{\mathrm{f}j} i_j + v_{\mathrm{pcc}} \tag{8}$$

Here, v_j and i_j represent the output voltage and output current measurements of converter j, respectively, while v_{pcc} is the voltage of the common DC Bus. Note that, unlike the implementation of RLS in AC microgrids [31], the proposed methodology in this paper only requires knowledge of the feeder resistances, and thus, (8) does not include any state variables.

Now, if we consider v_j and v_{pcc} as the system input variables and i_j as the output variable, Eq. (8) can express as follows:

$$i_j = \frac{1}{R_{\mathrm{f}j}}(v_j - v_{\mathrm{pcc}}) \tag{9}$$

Since the controller is implemented digitally, (9) can be written in discrete-time form as shown below:

$$i_j(k) = \frac{1}{R_{\mathrm{f}j}}\left[v_j(k) - v_{\mathrm{pcc}}(k)\right] \tag{10}$$

where (k) represents a sample of a measured variable.

As (10) is written in a linear regression form, $R_{\mathrm{f}j}$ can be computed online using the RLS algorithm based on the three available measured quantities (v_j, i_j and v_{pcc}). Then, the estiamted feeder resistance ($\hat{R}_{\mathrm{f}j}$) in real-time by each converter controller will be used to tune the virtual resistance ($R_{\mathrm{v}j}$) as described next. Eq. (10) highlights that the proposed approach has a low computational cost as the calculation steps for resistance estimation are recursively executed at every sample instance (k) of the controller (20 kHz) [33], where only three measurements (v_j, i_j and v_{pcc}) are required to be processed.

It is worth mentioning that the RLS estimation algorithm is only necessary for initializing the feeder resistances. After the estimation process, the RLS algorithm can be disabled, and the estimated values can be stored and used in the proposed control law, as presented in (11). Moreover, if the resistance values of the feeders are known from the design stage, there is no need to use the RLS algorithm, and the known values can be directly fed into the proposed control law to tune the virtual resistances.

3.2. Optimal tuning of the virtual resistances

The online tuning procedure for derermining the optimal virtual resistances ($R_{\mathrm{v}1}, R_{\mathrm{v}2}, \ldots$) is based on the estimated feeder resistances ($\hat{R}_{\mathrm{f}1}, \hat{R}_{\mathrm{f}2}, \ldots$). The proposed concept is explained using the simple system depicted in Fig. 3.

Given that $R_{\mathrm{f}1} > R_{\mathrm{f}2}$ and $R_{\mathrm{f}1} > R_{\mathrm{f}3}$, the base case is established with converter 1 and the virtual resistance of converter 1, $R_{\mathrm{v}1}$, is set to zero in order to prevent large unnecessary output voltage deviations among the converters. Next, the estimated value of the base case, which in this scenario represents the feeder 1 resistance ($\hat{R}_{\mathrm{f}1}$), is shared with the other converters existing in the microgrid (here, converter 2 and converter 3).

Finally, the virtual resistances of converter 2 and converter 3 ($R_{\mathrm{v}2}$, $R_{\mathrm{v}3}$) are set proportionally to the differences between their respective estimated feeder resistances and the shared feeder 1 resistance. The control law for optimizing virtual resistances to be used in (7) for the microgrid shown in Fig. 3 is summarized as follows:

$$\begin{cases} R_{\mathrm{v}1} = 0 \\ R_{\mathrm{v}2} = (\hat{R}_{\mathrm{f}1} - \hat{R}_{\mathrm{f}2}) \\ R_{\mathrm{v}3} = (\hat{R}_{\mathrm{f}1} - \hat{R}_{\mathrm{f}3}) \end{cases} \tag{11}$$

where $R_{\mathrm{v}1}$, $R_{\mathrm{v}2}$, and $R_{\mathrm{v}3}$ are the proposed virtual resistance values for converter 1, converter 2, and converter 3, respectively. $\hat{R}_{\mathrm{f}1}$, $\hat{R}_{\mathrm{f}2}$, and $\hat{R}_{\mathrm{f}3}$ are the resistance values of feeder 1, feeder 2, and feeder 3, respectively, estimated using (10). Consequently, $R_{\mathrm{v}2}$ is embedded into the control loop of converter 2 to modify its output voltage reference value according to (7). Similarly, $R_{\mathrm{v}3}$ modifies the output voltage reference value for converter 3, and so on. As a result, the voltage drops across the microgrid feeders with the proposed virtual resistances are equal, and accurate power sharing among converters is achieved. The voltage drops between the output of each converter and the DC Bus after enabling the proposed control strategy are expressed in (12).

$$\begin{cases} R_{\mathrm{f}1} i_1 = (R_{\mathrm{f}2} + R_{\mathrm{v}2}) i_2 = (R_{\mathrm{f}3} + R_{\mathrm{v}3}) i_3 \\ P_{\mathrm{pcc}1} = P_{\mathrm{pcc}2} = P_{\mathrm{pcc}3} \end{cases} \tag{12}$$

Fig. 4 shows the detailed implementation of the proposed virtual resistance tuning for converter j, along with the online resistance estimation of feeder j using the RLS algorithm.

One of the main advantages of the proposed control strategy is its reliability in the case of communication failures. If the communication between the secondary control and primary control layers fails, the proposed control strategy ensures that each converter supplies the same amount of power to the load, with only a minor mismatch of the total delivered power to the load from its desired reference occurring due to the absence of the secondary control layer. Moreover, the proposed virtual resistance for each converter does not require retuning after the communication is lost, making the proposed control strategy robust toward communication disruptions and delays.

4. Results

In this section, simulations and experimental results based on hardware-in-the-loop (HIL) are presented to validate the performance of the proposed control scheme.

4.1. Simulation results

4.1.1. Converters with equal power rating

To demonstrate the efficacy of the proposed control strategy, the islanded DC microgrid consisting of three converters, shown in Fig. 3, is considered. The system is implemented in MATLAB/Simulink software. Table 1 lists the system parameters used in the simulations. In the simulation, the performance of the system is tested under four different conditions as follows:

1. Test 1 ($0 \leq t < 1$ s): the system operation without virtual resistance (annotated in the figure as conventional control) is examined for a microgrid load equal to $P_{\mathrm{load}} = 6$ kW.
2. Test 2 ($t \geq 1$ s): the system operation under the proposed control is tested, where the virtual resistances of converters 2 and 3 are set according to (11).
3. Test 3 ($t \geq 2$ s): a step change in the microgrid load, P_{load}, from 6 kW to 9 kW is applied under the proposed control.
4. Test 4 ($t \geq 3$ s): a communication loss is simulated under the proposed control.

Fig. 5 illustrates the power consumed by the load and the power delivered to the load by each converter. When conventional control (without virtual resistance) is applied ($0 \leq t < 1$ s), even though the 6 kW load demand is met, each identical converter delivers a different power to the load due to mismatched feeder resistance values. The power at the PCC for each converter is $P_{\mathrm{pcc}1} = 0.814$ kW, $P_{\mathrm{pcc}2} = 1.672$ kW and $P_{\mathrm{pcc}3} = 3.514$ kW.

When the proposed control is enabled at $t = 1$ s, Fig. 5 shows that each converter delivers 2 kW to the load, achieving the desired objective of equal power sharing. This goal is met even when the load at the DC Bus increases to 9 kW at $t = 2$ s, and each converter delivers 3 kW to the load. In the case of communication failure (i.e., secondary control disabled), $t \geq 3$ s, the power sharing among converters remains

Table 1
Simulation parameters of the system.

Quantity	Symbol	Value	Unit
Microgrid			
Nominal voltage	v^*_{DC}	400	V
Initial load power	P_{L1}	6	kW
Final load power	P_{L2}	9	kW
Resistance of feeder 1	R_{f1}	0.2	Ω
Resistance of feeder 2	R_{f2}	0.1	Ω
Resistance of feeder 3	R_{f3}	0.05	Ω
DC boost converters 1, 2 and 3			
Nominal power	P_{rated}	5	kW
Nominal voltage	v_{rated}	400	V
Nominal current	i_{rated}	12.5	A
Switching frequency	f_{sw}	10	kHz
Control parameters for individual DC boost converter			
Current controller			
Proportional gain	K_{p-cc}	7	Ω
Integral gain	K_{i-cc}	100	Ω/s
Voltage controller			
Proportional gain	K_{p-vc}	1	S
Integral gain	K_{i-vc}	500	S/s
Secondary control of the microgrid			
Proportional gain	K_{p-sec}	1	-
Integral gain	K_{i-sec}	100	1/s

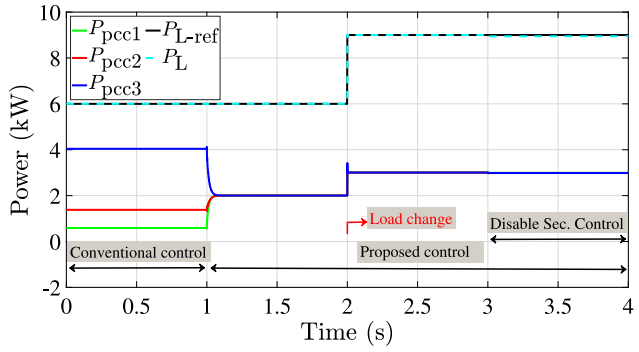

Fig. 5. Load power sharing among the three DC–DC converters under the conventional control without virtual resistance for $0 \le t < 1$ s, and under the proposed control for $1 \le t \le 4$ s.

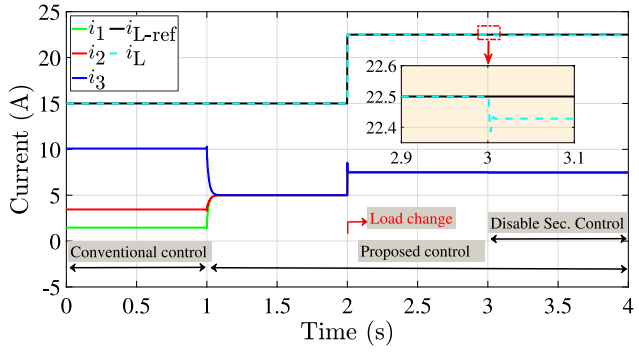

Fig. 6. Microgrid current waveforms.

equal, although a slightly decreased amount of power is delivered to the load.

Fig. 6 illustrates the current waveforms in the microgrid. As shown in the figure, under the traditional control scheme for $0 \le t < 1$ s, the magnitude of currents of the three converters are not identical. However, after enabling the proposed control for $t \ge 1$ s, the current waveforms of the three converters have identical magnitudes, which indicates the successful achievement of balanced current sharing.

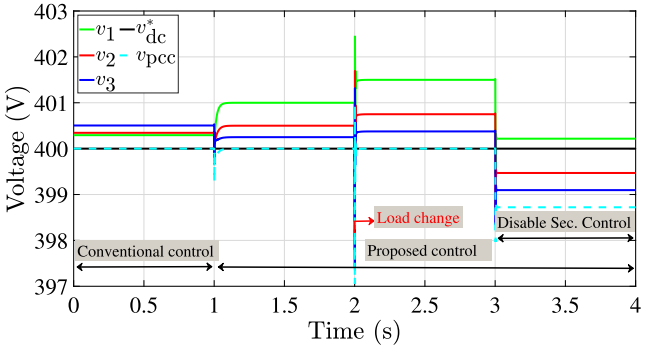

Fig. 7. Output voltages of the three converters and voltage of the microgrid load.

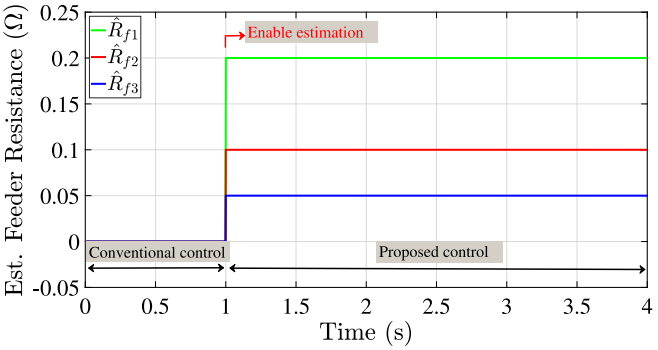

Fig. 8. Online estimation of the resistances of feeder 1, 2, and 3 by converters 1, 2, and 3, respectively.

Fig. 7 presents the output voltages of the three converters. As observed in the figure, under the proposed control with the optimally tuned virtual resistance for $t \ge 1$ s, the voltage of converter 1 (v_1) is the highest. This can be attributed to the larger resistance value of feeder 1 compared to feeders 2 and 3. Moreover, Fig. 7 displays the voltage amplitude of the microgrid load and its reference. It can be observed that by adopting the secondary control loop, the microgrid voltage is regulated to its nominal value of 400 V as listed Table 1.

Fig. 8 depicts the online estimation results of the feeder resistance by converter 1. The RLS algorithm provides accurate estimation results of the resistances after it was enabled at $t \ge 1$ s. Notably, the RLS estimation algorithm is only required to initialize the feeder resistances. Once estimated, the values are held and used in the proposed control law presented in (11).

4.1.2. Performance of proposed controller during faults

In order to further validate the reliability of the proposed control strategy, a sudden loss of converter 3 at 1.5 s is tested. The results of this test are shown in Fig. 9. The proposed controller ensures accurate load power sharing between converters 1 and 2 even after the loss of converter 3 at $t \ge 1.5$ s. As an example, the 6 kW load power is distributed equally between converters 1 and 2. Furthermore, even when the load changes from 6 kW to 9 kW at $t \ge 2$ s, and with converter 3 is out of service, converters 1 and 2 share the load power equally. This desirable performance further confirms the robustness of the proposed power sharing control under abnormal operating conditions.

4.1.3. Accuracy of the estimated resistances using the RLS algorithm

The accuracy of the estimated resistance using the RLS algorithm is tested in three conditions. While the first condition considers the RLS parameter (forgetting factor λ), the second and third conditions investigate the effects of the communication delays in the MG links and measurements noise.

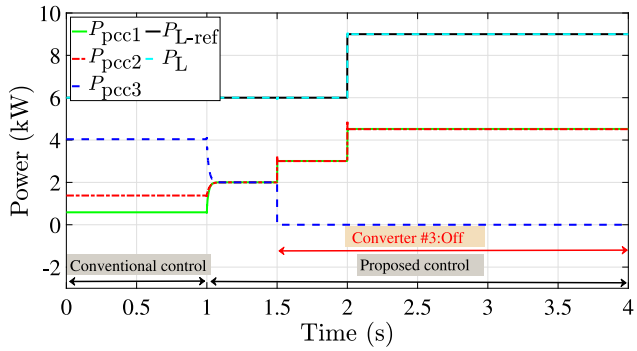

Fig. 9. Load power sharing in the DC microgrid under the proposed control following disconnection of converter 3 at $t \geq 1.5$ s.

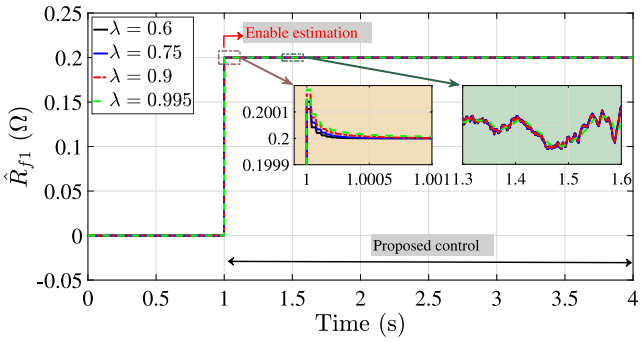

Fig. 10. Variation of the estimated resistance of feeder 1 for varying the forgetting factor λ value of the RLS algorithm.

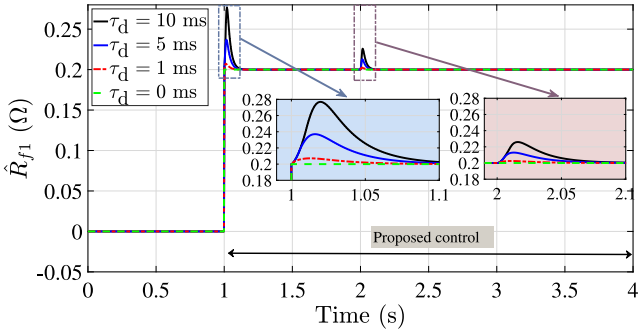

Fig. 11. Variation of the estimated resistance of feeder 1 by the RLS algorithm considering communication delays.

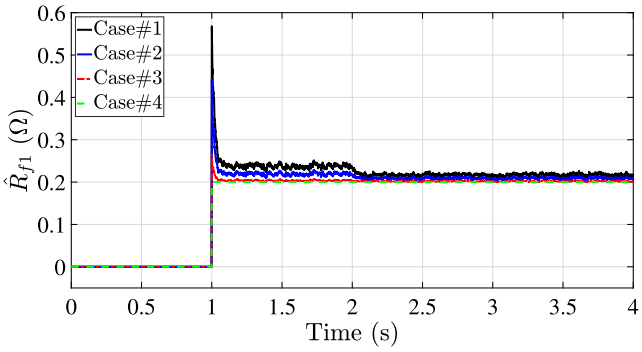

Fig. 12. Variation of the estimated resistance of feeder 1 by the RLS algorithm considering measurement noise.

1. Effects of the forgetting factor of the RLS algorithm
   For the online estimation of the feeders resistances, the influence of the forgetting factor (λ) of the RLS algorithm is evaluated first. The performance of the RLS algorithm is significantly impacted by the selection of λ. As shown in Fig. 10, the estimation results of $\hat{R}_{f1}$ by converter 1 using different values for λ illustrate a tradeoff between stability and tracking ability. The RLS algorithm achieves good stability for λ values closer to unity. However, the tracking capability of the algorithm is reduced [33]. Therefore, in this paper, $\lambda = 0.995$ is chosen.
2. Effects of communication delays
   Communication delays are inherent in practical applications of hierarchical control in microgrids, regardless of whether they use low or high-bandwidth communication networks. These delays can cause control signals sent from the secondary control to be delayed or lost in transmission, potentially impacting microgrid stability and security in the worst case scenario [35]. To evaluate the robustness of the proposed secondary control, the microgrid performance is investigated for a range of communication time delays [0, 1, 5, 10 ms]. Fig. 11. shows the estimated resistance of feeder 1 after enabling the RLS estimation algorithm at $t = 1$ s, with the different values of communication delay (τ_d). It can be observed that the four different values of communication delay affect only the transients, and the steady state estimation results are robust. However, Fig. 11 shows that increasing communication delays are associated with larger transients.
3. Effects of measurement noise
   In order to evaluate the accuracy of the estimated resistances using the RLS algorithm, white noise with different amplitudes is added to the measurements. Fig. 12 shows the obtained results, where cases 1, 2, and 3 represent estimated resistance with noise amplitudes of approximately 2, 1, and 0.5 V, respectively. Case 4 represents the ideal estimation with no noise. It is evident that good estimation results are still obtained even in the presence of noise.

4.1.4. Comparison with fixed virtual resistances method

The advanced control methods discussed in the Introduction, such as centralized, distributed, and consensus-based algorithms, can ensure highly accurate results, but they are often complicated and cannot guarantee accurate power sharing during faults, such as communication loss and sudden converter shutdown. In contrast, although it can cause significant degradation of the PCC voltage, the fixed virtual resistance method remains one of the most commonly used power sharing methods in the literature and can still be effective during fault events. Therefore, this section compares the proposed method with the fixed virtual resistance control method since they can both work during faults. However, the proposed method outperforms the fixed virtual resistance method, delivering superior performance and achieving more accurate power sharing.

In the fixed virtual resistance method, it is suggested that the values assigned to the virtual resistances should be greater than the maximum expected feeder resistance to minimize the negative impact of mismatched feeder resistances. To make the comparison in this section, three DC–DC converters are simulated in which their virtual resistances are set to the same value equal to five times the maximum feeder resistance, $5R_{f1}$.

Fig. 13(a) and Fig. 13(b) show the obtained results with no virtual resistance for $t < 1$ s and with fixed virtual resistance for $t \geq 1$ s. It can be observed that the control scheme with fixed virtual resistance fails to ensure zero steady-state errors in the load power sharing between the three identical DC–DC converters due to the mismatched feeder resistances. Furthermore, the load voltage drops after disabling the

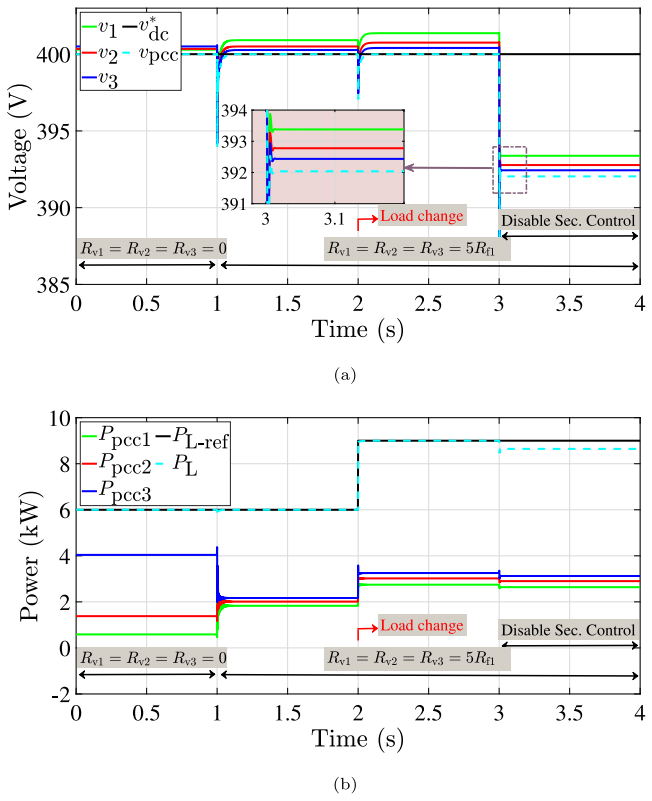

Fig. 13. Performance of the DC microgrid with the fixed virtual resistance control approach ($R_{vj} = 5R_{f1}$) without virtual resistance for $0 \le t < 1$ s, and with fixed virtual resistances for $1 \le t \le 4$ s: (a) Microgrid voltages (b) Power at the PCC.

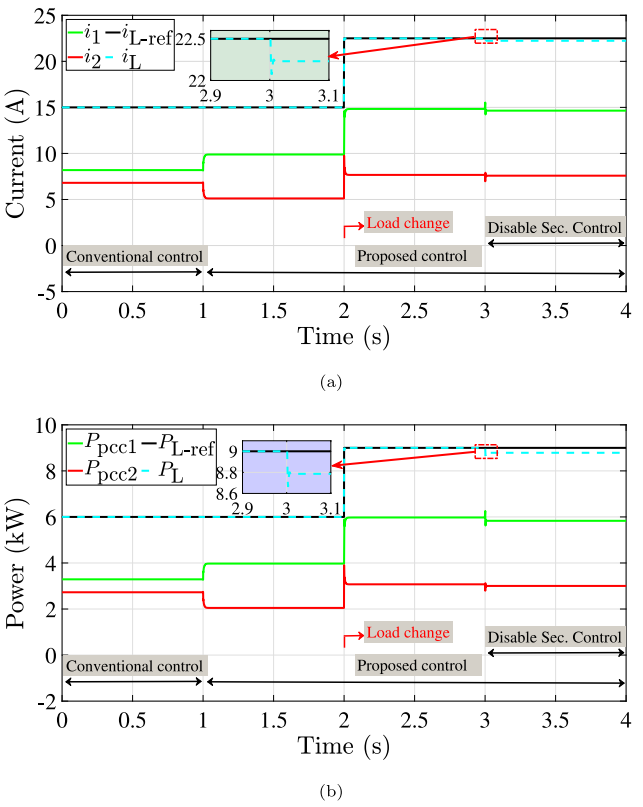

Fig. 14. Performance of the DC microgrid with nonidentical DC converters, $P_{rated1} = 2P_{rated2} = 10$ kW, without virtual resistance for $0 \le t < 1$ s, and with the proposed virtual resistances for $1 \le t \le 4$ s: (a) Microgrid current (b) Power at the PCC.

secondary control at $t = 3$ s to 392 V, which is much larger than that value of 398.7 V for the proposed controller shown in Fig. 7.

4.1.5. Converters with different power rating

While all case studies reported in this paper consider the converters with the same power rating of 5 kW, this case study considers non-identical converters with different power ratings. Two converters are considered, where the power rating of the second converter is half of that of converter 1, $P_{rated2} = 0.5P_{rated1} = 5$ kW. Therefore, an additional loop is required to implement the primary droop control. In this loop, the output current is multiplied by the droop coefficients (m_j), and the output is subtracted from the reference voltage of the inner voltage loop, v^*_{DCj}. The droop coefficient (m_j) for each converter is calculated based on its rated current and the maximum allowable voltage deviations, $m_j = \delta v\text{dc}/i_{\text{ratedj}}$ [9]. Assuming the maximum allowable voltage deviation is 1% voltage and the maximum/rating current for converters 1 and 2 are 25 and 12.5 A at the rating voltage of 400 V, then $m_1 = 0.16$ and $m_1 = 0.32$, respectively.

In this case study, the feeders resistances are not identical and are equal to the values listed in Table 1. Ideally, the injected power/current by converter 2 should be half that of converter 1. To accomplish this, the virtual resistance value of converter 2 is increased twofold from the value calculated in (11).

Fig. 14 shows the current and power sharing between converters 1 and 2. It can be observed that the conventional control ($t < 1$ s) fails to ensure proportional current and power sharing. However, once the proposed control is activated at $t = 1$ s, the power sharing of the load between the two nonidentical DC–DC converters is achieved accurately and proportionally to their power rating. For instance, when the load power is 9 kW for $t \ge 2$ s, converters 1 and 2 supplied 3 and 6 kW, respectively.

4.2. Hardware-in-the-loop experimental results

To further validate the power sharing performance of the proposed strategy, hardware-in-the-loop (HIL) experiments were conducted. The investigated DC microgrid consisted of two identical DC boost converters. As shown in the block diagram in Fig. 15, the PLECS RT Box from PLEXIM was used to emulate the power stage of the circuit, while the TMS320F28069M LaunchPad from Texas Instruments was used for real-time implementation of the control algorithm. The parameters of the HIL test bench were selected to be identical to those employed in the simulations presented in Table 1, except for the feeder resistance values, which were here increased fivefold relative to the values listed in Table 1.

In this section, two different cases have been investigated and tested with different line resistances for feeders 1 and 2. In Case 1, the power sharing between the two boost converters was considered while supplying a common 8 kW microgrid load. In Case 2, an abnormal operation scenario was tested with the loss of communication links between the MGCC and the local controllers of the two boost converters.

4.2.1. Case 1 - Load power sharing

Considering that the load power is 8 kW and both boost converters have the same power ratings of 5 kW, it is expected that each converter would supply the load with 4 kW. However, as shown in Fig. 16, the load power sharing is poor under the conventional control strategy, with each converter outputting a different power level. The first converter supplies only 2.6 kW due to its large feeder resistance, while the second converter is heavily loaded with 5.4 kW due to its small feeder resistance. At time instant t_1, marked by the red vertical line in the figure, the proposed control strategy is enabled, whereby the virtual resistance of the second converter is deployed to compensate

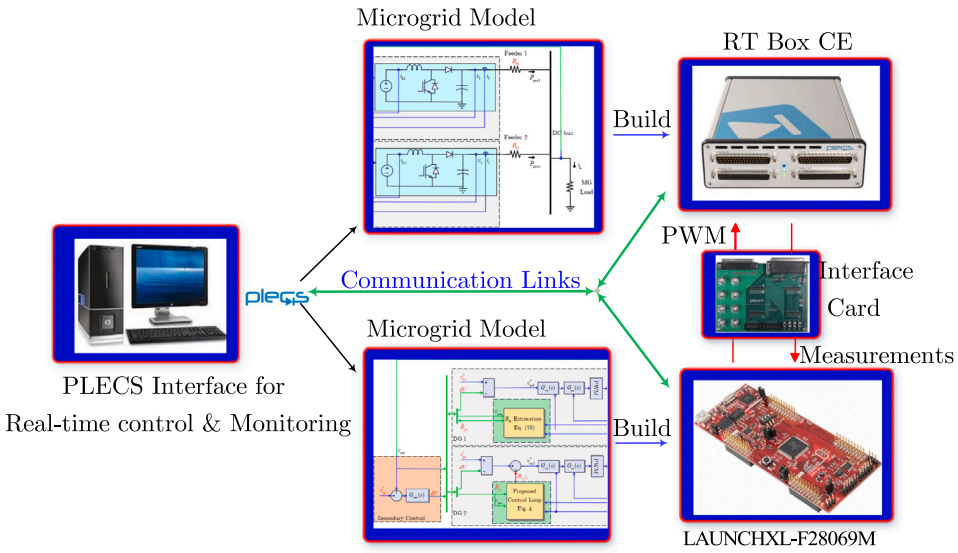

(a)

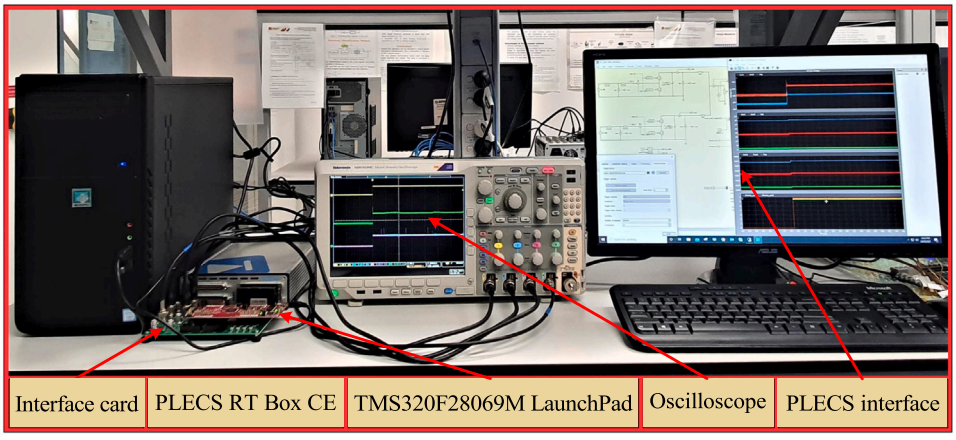

(b)

Fig. 15. Hardware-in-the-loop setup: (a) Block diagram of the setup, (b) Screenshot of the setup.

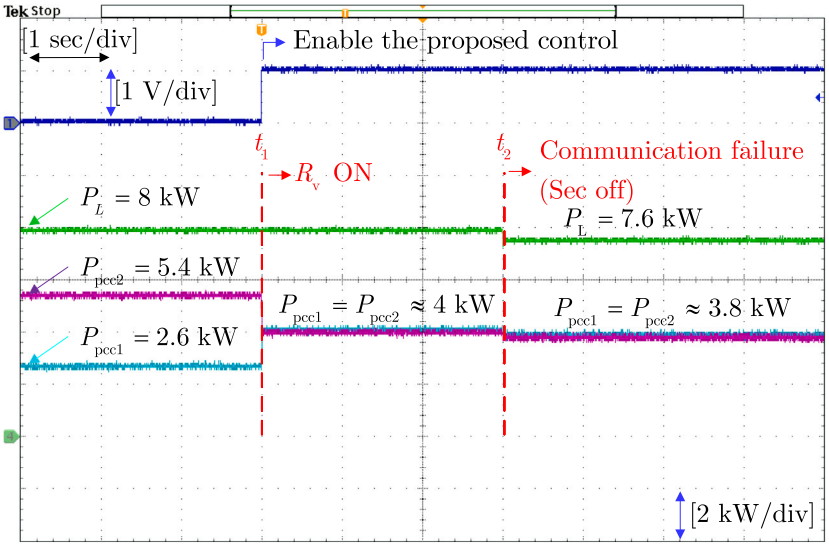

Fig. 16. Experimental results of the power sharing under the conventional and the proposed control methods.

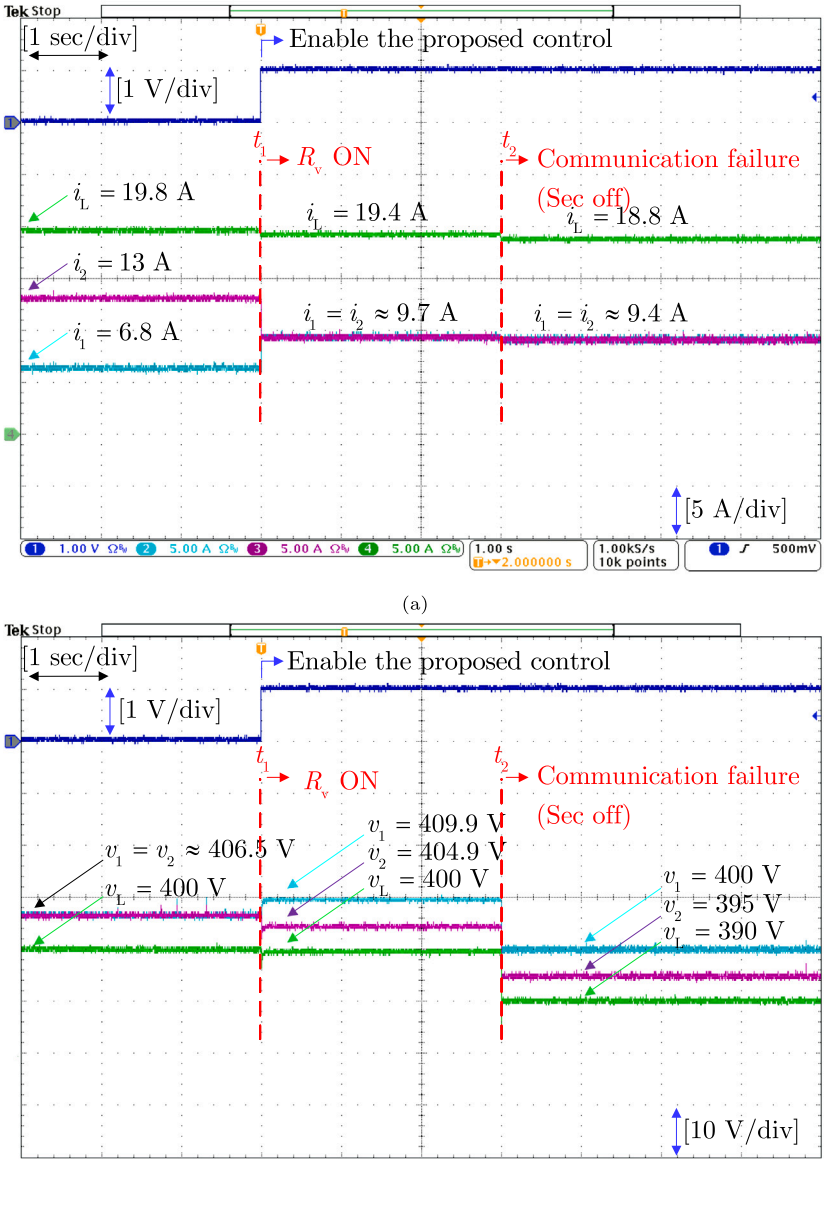

Fig. 17. Experimental results of the microgrid current and voltage under the conventional and the proposed control methods: (a) current, (b) voltage.

for the mismatched resistance of the microgrid feeders. This leads to equalization of the PCC power of both converters for $t > t_1$.

Fig. 17(a) illustrates the output current sharing between the two boost converters and the microgrid load current. The conventional control strategy shows unequal current sharing between converters, with converter 1 supplying 6.8 A and converter 2 heavily loaded with 13 A for $t < t_1$. However, after enabling the proposed control strategy for $t \geq t_1$, both converters share the load current equally, with each supplying around 9.7 A to the load.

Fig. 17(b) depicts the terminal voltage of both converters and the DC Bus voltage. The conventional control strategy, for $t < t_1$, maintains the terminal voltages of converters 1 and 2 equal to 406.5 V. Upon enabling the proposed control strategy for $t \geq t_1$, these voltages are set automatically to different values, fully compensating for the mismatch in the value of feeder resistances.

4.2.2. Case 2 - Loss of communication links

For $t \geq t_2$, Fig. 16 and Fig. 17demonstrate the experimental results where loss of communication links between the secondary controller and the two DC–DC converters occurred. Despite a slight drop in the overall power supplied to the load, from 8 kW to 7.6 kW, and the DC Bus voltage settling 10 V below its reference value, equal current sharing between converters 1 and 2 is maintained despite the communication link failure. This is possible because the local controller of each converter uses the virtual resistance values assigned before the communication failure, and there is no need to retune these virtual resistances when communication is lost. Hence, the proposed control strategy has the added advantage of being reliable under such abnormal operating conditions.

It is worth noting a related concern regarding the microgrid architecture examined in this paper, in which converters supply power to a central load (as shown in Fig. 3). This architecture was chosen as it is commonly used in the literature to evaluate power sharing accuracy and the performance of secondary control in converter-based microgrids [9]. Future research could explore alternative microgrid architectures, including mesh-type and interconnected DC microgrids.

5. Conclusion

In this paper, a strategy for achieving accurate load power sharing for islanded DC microgrids is proposed. This strategy involves two main stages. First, an online estimation of the feeder resistances is performed using the recursive least squares algorithm, which is implemented into the local controller of each converter. This avoids the need for prior knowledge of the actual feeder resistances in the design stage. Second, the estimated feeder resistances are used to optimally tune the virtual resistance assigned to each converter in the microgrid, resulting in proportional load power sharing among converters and avioding undesired voltage degradation in the DC microgrid. Moreover, the proposed technique is fault-tolerant as it ensures accurate power sharing among the converters even under permanent communication failure between the microgrid central controller and the local controllers of the converters. The simplicity, software-based implementation, and utilization of only available measurements make the proposed control strategy suitable for enhancing the performance of both new and existing DC microgrids.

CRediT authorship contribution statement

Nabil Mohammed: Conceptualization, Methodology, Software, Validation, Formal analysis, Writing – original draft, Investigation, Writing – review & editing, Visualization. **Leonardo Callegaro:** Formal analysis, Writing – review & editing, Visualization. **Mihai Ciobotaru:** Methodology, Resources, Writing – review & editing, Supervision, Project administration. **Josep M. Guerrero:** Writing – review & editing, Visualization.

Data availability

No data was used for the research described in the article

References

[1] Ackermann T, Andersson G, Söder L. Distributed generation: a definition. Electr Power Syst Res 2001;57(3):195–204.

[2] Lasseter RH. Microgrids. In: 2002 IEEE power engineering society winter meeting. Conference proceedings (Cat. No. 02CH37309), vol. 1. IEEE; 2002, p. 305–8.

[3] Balog RS, Weaver WW, Krein PT. The load as an energy asset in a distributed DC smartgrid architecture. IEEE Trans Smart Grid 2011;3(1):253–60.

[4] Dragičević T, Lu X, Vasquez JC, Guerrero JM. DC microgrids—Part I: A review of control strategies and stabilization techniques. IEEE Trans Power Electron 2015;31(7):4876–91.

[5] Dragičević T, Lu X, Vasquez JC, Guerrero JM. DC microgrids—Part II: A review of power architectures, applications, and standardization issues. IEEE Trans Power Electron 2016;31(5):3528–49.

[6] Zhao J, Dörfler F. Distributed control and optimization in DC microgrids. Automatica 2015;61:18–26.

[7] Fletcher SD, Norman PJ, Galloway SJ, Crolla P, Burt GM. Optimizing the roles of unit and non-unit protection methods within DC microgrids. IEEE Trans Smart Grid 2012;3(4):2079–87.

[8] Han Y, Ning X, Yang P, Xu L. Review of power sharing, voltage restoration and stabilization techniques in hierarchical controlled DC microgrids. IEEE Access 2019;7:149202–23.

[9] Guerrero JM, Vasquez JC, Matas J, De Vicuña LG, Castilla M. Hierarchical control of droop-controlled AC and DC microgrids—A general approach toward standardization. IEEE Trans Ind Electron 2010;58(1):158–72.

[10] Lu X, Guerrero JM, Sun K, Vasquez JC. An improved droop control method for DC microgrids based on low bandwidth communication with DC bus voltage restoration and enhanced current sharing accuracy. IEEE Trans Power Electron 2013;29(4):1800–12.

[11] da Silva WWA, Oliveira TR, Donoso-Garcia PF. Hybrid distributed and decentralized secondary control strategy to attain accurate power sharing and improved voltage restoration in DC microgrids. IEEE Trans Power Electron 2019;35(6):6458–69.

[12] Fan B, Guo S, Peng J, Yang Q, Liu W, Liu L. A consensus-based algorithm for power sharing and voltage regulation in DC microgrids. IEEE Trans Ind Informat 2019;16(6):3987–96.

[13] Lu X, Guerrero JM, Sun K, Vasquez JC, Teodorescu R, Huang L. Hierarchical control of parallel AC-DC converter interfaces for hybrid microgrids. IEEE Trans Smart Grid 2013;5(2):683–92.

[14] Anand S, Fernandes BG, Guerrero J. Distributed control to ensure proportional load sharing and improve voltage regulation in low-voltage DC microgrids. IEEE Trans Power Electron 2012;28(4):1900–13.

[15] Dam D-H, Lee H-H. A power distributed control method for proportional load power sharing and bus voltage restoration in a DC microgrid. IEEE Trans Ind Appl 2018;54(4):3616–25.

[16] Huang P-H, Liu P-C, Xiao W, El Moursi MS. A novel droop-based average voltage sharing control strategy for DC microgrids. IEEE Trans Smart Grid 2014;6(3):1096–106.

[17] Nasirian V, Davoudi A, Lewis FL, Guerrero JM. Distributed adaptive droop control for DC distribution systems. IEEE Trans Energy Convers 2014;29(4):944–56.

[18] Fan B, Yang Q, Jagannathan S, Sun Y. Output-constrained control of nonaffine multiagent systems with partially unknown control directions. IEEE Trans Autom Control 2019;64(9):3936–42.

[19] Xie W, Han M, Cao W, Guerrero JM, Vasquez JC. System-level large-signal stability analysis of droop-controlled DC microgrids. IEEE Trans Power Electron 2020;36(4):4224–36.

[20] Xie W, Han M, Cao W, Guerrero JM, Vasquez JC. Virtual resistance tradeoff design for DCMG grid-forming converters considering static-and large-signal dynamic constraints. IEEE Trans Power Electron 2020;36(5):5582–93.

[21] Wang H, Han M, Han R, Guerrero JM, Vasquez JC. A decentralized current-sharing controller endows fast transient response to parallel DC–DC converters. IEEE Trans Power Electron 2017;33(5):4362–72.

[22] Wang P, Lu X, Yang X, Wang W, Xu D. An improved distributed secondary control method for DC microgrids with enhanced dynamic current sharing performance. IEEE Trans Power Electron 2015;31(9):6658–73.

[23] Zaery M, Ahmed EM, Orabi M, Youssef M. Operational cost reduction based on distributed adaptive droop control technique in DC microgrids. In: 2017 IEEE energy conversion congress and exposition (ECCE). IEEE; 2017, p. 2638–44.

[24] Xu Q, Xiao J, Hu X, Wang P, Lee MY. A decentralized power management strategy for hybrid energy storage system with autonomous bus voltage restoration and state-of-charge recovery. IEEE Trans Ind Electron 2017;64(9):7098–108.

[25] Mi Y, Guo J, Yu S, Cai P, Ji L, Wang Y, Yue D, Fu Y, Jin C. A power sharing strategy for islanded DC microgrid with unmatched line impedance and local load. Electr Power Syst Res 2021;192:106983.

[26] Cingoz F, Elrayyah A, Sozer Y. Optimized settings of droop parameters using stochastic load modeling for effective DC microgrids operation. IEEE Trans Ind Appl 2016;53(2):1358–71.

[27] Hoang KD, Lee H-H. Accurate power sharing with balanced battery state of charge in distributed DC microgrid. IEEE Trans Ind Electron 2018;66(3):1883–93.

[28] Anand S, Fernandes BG, Guerrero J. Distributed control to ensure proportional load sharing and improve voltage regulation in low-voltage DC microgrids. IEEE Trans Power Electron 2012;28(4):1900–13.

[29] Augustine S, Mishra MK, Lakshminarasamma N. Adaptive droop control strategy for load sharing and circulating current minimization in low-voltage standalone DC microgrid. IEEE Trans Sustain Energy 2014;6(1):132–41.

[30] Yuan C. Resilient distribution systems with community microgrids (Ph.D. thesis), The Ohio State University; 2016.

[31] Mohammed N, Ciobotaru M. An accurate reactive power sharing strategy for an Islanded microgrid based on online feeder impedance estimation. In: IECON 2020 the 46th annual conference of the IEEE industrial electronics society. IEEE; 2020, p. 2525–30.

[32] Han Y, Li H, Shen P, Coelho EAA, Guerrero JM. Review of active and reactive power sharing strategies in hierarchical controlled microgrids. IEEE Trans Power Electron 2016;32(3):2427–51.

[33] Paleologu C, Benesty J, Ciochina S. A robust variable forgetting factor recursive least-squares algorithm for system identification. IEEE Signal Process Lett 2008;15:597–600.

[34] Cobreces S, Bueno EJ, Pizarro D, Rodriguez FJ, Huerta F. Grid impedance monitoring system for distributed power generation electronic interfaces. IEEE Trans Ind Electron Contr Instrum 2009;58(9):3112–21.

[35] Coelho EA, Wu D, Guerrero JM, Vasquez JC, Dragicević T, Stefanović C, Popovski P. Small-signal analysis of the microgrid secondary control considering a communication time delay. IEEE Trans Ind Electron 2016;63(10):6257–69.